Assessment of interatomic potentials for molecular dynamics simulations of GaAs deposition

D. A. Murdick,* X. W. Zhou, and H. N. G. Wadley
Department of Materials Science and Engineering, School of Engineering and Applied Science, University of Virginia, Charlottesville, Virginia 22904, USA

(Received 16 March 2005; revised manuscript received 23 September 2005; published 30 November 2005)

Computational studies of atomic assembly processes during GaAs vapor deposition require interatomic potentials that are able to reasonably predict the structures and energies of a molecular arsenic vapor, a variety of elemental gallium and arsenic lattices, binary GaAs lattices, GaAs lattice defects, and (001) GaAs surfaces. These properties were systematically evaluated and compared to *ab initio* and experimental data for one Tersoff and two Stillinger-Weber (SW) GaAs interatomic potentials. It was observed that bulk and arsenic molecular properties calculated by the Tersoff parametrization matched density functional predictions and experimental observations significantly better than either of the SW parametrizations. These trends can be related to the bonding physics included in each potential format. Surface free energy calculations indicate that none of these potentials correctly predict the low-energy surface reconstructions of the GaAs (001) surface. Simulated As_2 molecular bonding with gallium-rich GaAs (001) surfaces indicate a high sticking probability for SW potentials, which is in good agreement with experimental observations at low growth temperatures. However, the Tersoff parametrization resulted in an unphysically high desorption probability for As_2 over a wide range of surface temperatures.

DOI: 10.1103/PhysRevB.72.205340 PACS number(s): 61.50.Ah, 81.05.Ea, 81.15.Aa, 61.50.Lt

I. INTRODUCTION

GaAs thin films are widely used in photonics, microelectronics, and the emerging field of spintronics. For example, GaAs heterostructures are used to create light-emitting diodes, lasers, infrared detectors, and solar cells.[1] Metal semiconductor field effect transistors (MESFETs) based on GaAs are an integral part of cellular phones and wireless communication products, direct broadcasting systems, global positioning systems, fiber optic drivers and receivers, and collision avoidance and phased array radars.[2] GaAs thin films doped with transition metals, such as manganese, have recently attracted considerable interest as ferromagnetic semiconductors for controlled spin injection applications.[3] These thin film devices are manufactured by vapor deposition methods. The processing conditions used to grow these thin films significantly influence defect concentrations,[4] crystallinity,[5] and growth stresses within the films.[6]

Various modeling and simulation techniques are being used to understand and improve the deposition processes used to make thin film structures. Continuum,[7–10] kinetic Monte Carlo (kMC),[11–15] density functional theory (DFT),[16–23] and hybrid DFT+kMC methods[24–27] have all been used to investigate bulk, defect, and surface properties as well as some aspects of GaAs vapor deposition.

Molecular dynamics (MD) with classical interatomic potentials provides a means to directly study the atomic assembly process. In MD simulations of vapor deposition, the Lagrangian of a grand canonical ensemble of atoms is numerically integrated at discrete time steps (typically about a femtosecond) to compute atom positions as a function of time.[28] The total number of atoms, N, whose position can be simulated depends on available computational resources and can range from thousands to tens of thousands, or even millions, of atoms.[29,30] Their motion can be predicted for simulation times that again depend on calculation resources, but can often extend to many nanoseconds.

The validity of MD simulations is largely determined by the potential energy function used to define interatomic interactions. The embedded atom method (EAM) potential has been widely used for close-packed metal systems.[31–34] A recent formalism that combines the EAM approach with a charge transfer potential has been proposed for the study of metal oxide compounds.[35] Semiconductors, with their highly covalent bonding, are more complex to model because they require angular dependent potentials. Many interatomic potentials and parametrizations have been proposed for GaAs.[36–46] Stillinger-Weber[47] (SW) and Tersoff potentials[48,49] have been widely used for studying the bulk properties of elemental semiconductors and their lattice defects.[50,51]

Simulating the atomic assembly of a thin film using MD methods is one of the most demanding uses of interatomic potentials. The potentials need to be carefully fitted to *ab initio* and experimental data in such a way that the bulk structures are modeled sufficiently well so that the lattice structure, cohesive energy, elastic constants, and defect energetics are well approximated. They must also correctly predict the energetics of the highly defective surface during the growth processes. An assessment of the many proposed GaAs potentials (see Appendix A) suggests that three potentials offer the most promise for simulating the vapor deposition of GaAs. The Tersoff potential[49,52,53] as parametrized by Albe *et al.*[45] (TR-ANNK) and the SW potential[47] as parametrized by Wang and Stroud[37] (SW-WS) and Angelo and Mills and Grein *et al.*[38,39] (SW-AMG+) are studied in detail. The utility of the various potentials and their parametrizations are systematically investigated for their ability to model GaAs properties. Particular attention is given to properties that affect thin film growth.

II. ATOMIC VOLUME AND COHESIVE ENERGY

During vapor deposition, deposited atoms and molecules sample many different bonding environments before finding

their final configuration. One useful way to assess a GaAs interatomic potential is to calculate the atomic volume and cohesive energy of various GaAs phases with coordinations from 4 to 12 and to compare these to experimental data and *ab initio* (DFT) calculations.

At atmospheric pressure and for temperatures below the melting temperature, the lowest-energy crystalline phase of GaAs has a zinc blende (zb) structure.[54,55] The lowest-energy solid structures (at low pressure) for pure gallium and arsenic are the orthorhombic αGa($A11, Cmca$) and the rhombohedral αAs($A7, R\bar{3}m$) crystal phases.[56] The zb atomic volume for GaAs is 22.46 Å^3/atom,[55] while the elemental phases have atomic volumes of 19.34 and 21.30 Å^3/atom for the αGa and αAs phases, respectively.[56] Lattice parameters for the elemental structures have been summarized by Donohue[56] as a function of temperature.

Enthalpies are measured experimentally with respect to standard temperature and pressure conditions for gallium, arsenic, and gallium arsenide phases.[57,58] Theoretical calculations based upon DFT or interatomic potentials are usually calculated under zero temperature and pressure conditions. These calculated relative energies, or cohesive energies, are reported as the energy difference between a collection of free atoms and the atoms bound in their lowest-energy solid phase. Comparison, with respect to the same reference state, can be made between experimental enthalpy (ΔH) and calculated energy (ΔE) values through the thermodynamic relation, $\Delta H = \Delta E + \Delta(PV)$, where P is the pressure and V is the volume of the system. The $\Delta(PV)$ term is usually small compared to ΔE for condensed matter systems at constant pressure in the free atom reference state. Hence, for a solid phase at a temperature (T), $\Delta H^T \approx \Delta E^T$ is a reasonable approximation. This approximation becomes exact at 0 K.

The experimental enthalpies at 298 K and atmospheric pressure are −6.690 eV per formula unit (fu) for GaAs, −2.819 eV/fu for gallium, and −3.135 eV/fu for arsenic, with respect to the free atom reference state.[58] The values for gallium and arsenic at 0 K have been reported as -2.812 ± 0.022 eV/fu and -2.959 ± 0.026 eV/fu, respectively.[59] For GaAs, the conversion from 298 K ($\Delta H^{298\ \mathrm{K}}$) to 0 K ($\Delta H^{0\ \mathrm{K}}$) can be performed by integrating the constant pressure specific heat, ΔC_p, with respect to temperature[60]

$$\Delta E^{0\mathrm{K}} = \Delta H^{0\mathrm{K}} = \Delta H^{298\mathrm{K}} - \int_{0\mathrm{K}}^{298\mathrm{K}} \Delta C_p(T)\,dT, \qquad (1)$$

where $\Delta C_p(T) = C_p^{\mathrm{GaAs}(s)}(T) - C_p^{\mathrm{Ga}(g)}(T) - C_p^{\mathrm{As}(g)}(T)$. The specific heat of each component must be accounted for when calculating the enthalpy at 0 K. Data for $C_p^{\mathrm{GaAs}(s)}(T)$ have been tabulated by Adachi,[61] and specific heats for gallium and arsenic gases can be derived assuming an ideal gas.[57] This results in an enthalpy temperature correction of $\int_0^{298} \Delta C_p(T)\,dT \approx 0.030$ eV/fu. The change in GaAs enthalpy from 298 K to 0 K is less than 1%. Likewise, for elemental gallium and arsenic, the change in enthalpy between 298 K and 0 K is less than 1% for gallium and about 6% for arsenic. This is within the uncertainty in the calculation of cohesive energy for most DFT methods.[62] Therefore, for simplicity and source consistency, the cohesive energies (E) are approximated here using the enthalpy data at 298 K as: $E_{\mathrm{GaAs}} = -6.690$ eV/fu, $E_{\mathrm{Ga}} = -2.819$ eV/fu, and $E_{\mathrm{As}} = -3.135$ eV/fu.[58]

The crystal structures used to evaluate the potentials' bulk properties are identified using the common name, *Stukturbericht* designation, Pearson symbol, and space group notation.[55,63,64] The atomic volume and cohesive energies have been calculated for the zb ($B3, cF8, F\bar{4}3m$), NaCl ($B1, cF8, Fm\bar{3}m$), NiAs ($B8, hP4, P6_3/mmc$), and CsCl ($B2, cP2, Pm\bar{3}m$) structures of GaAs using the local density approximation (LDA) DFT method.[65] The elemental diamond cubic (dc) ($A4, cF8, Fd\bar{3}m$), face-centered cubic (fcc) ($A1, cF4, Fm\bar{3}m$), simple cubic (sc) ($A_h, cP1, Pm\bar{3}m$), body-centered cubic (bcc) ($A2, cI2, Im\bar{3}m$), Ga-II ($cI12, I\bar{4}3d$), αGa($A11, oC8, Cmca$), and αAs($A7, hR2, R\bar{3}$) structure parameters and energies were calculated in a similar manner by Albe *et al.*[45] for gallium and arsenic. The cohesive energies for elemental gallium and arsenic were calculated relative to αGa and αAs structures.

LDA data as not given by Albe *et al.*[45] for the gallium bcc structure. However, the generalized gradient approximation (GGA) data of Baskes *et al.* is available.[66] The energy and volume data predicted by the LDA and GGA methods for αGa, dc, fcc, and sc structures can be directly compared, if the GGA DFT atomic volume is scaled by 90% and the bcc cohesive energy (relative to the lowest-energy phase) is scaled by 120%. The approximated values of LDA-equivalent gallium bcc data are −2.758 eV/atom for cohesive energy and 17.520 Å^3 for atomic volume. These values are sufficiently accurate for producing a qualitative trend in energies and volumes.

The predicted atomic volumes and cohesive energies using the three potentials were determined using molecular statics methods described in Appendix B. Figure 1 shows a comparison of the calculated, experimental, and DFT data. It can be seen that the SW-WS potential consistently overestimated the atomic volume (by about 160%) and underestimated the cohesive energy by ~50% for all the phases evaluated. The SW-AMG+ potential overestimated the arsenic atomic volume (by 120–180%) and underestimated the elemental cohesive energies (by 11–64%). The TR-ANNK potential closely matched both experimental and DFT data.

The cohesive energy and atomic volume of crystalline structures predicted by each potential provided insight about the gallium and arsenic atom response to changes in homopolar or heteropolar bonding environments. The arsenic and gallium elemental results indicate that homopolar bonds were not well modeled by either of the SW parametrizations (Fig. 1). The lowest-energy phases for gallium and arsenic were predicted to be either tetrahedral dc (SW-WS, As, and Ga; SW-AMG+, Ga) or close-packed fcc (SW-AMG+, As) structures. Neither of these predicted structures match the experimentally observed crystalline structure of αGa or the buckled planes of αAs.[56]

Clearly, care needs to be taken when using either of the SW parametrizations to model processes that require an ac-

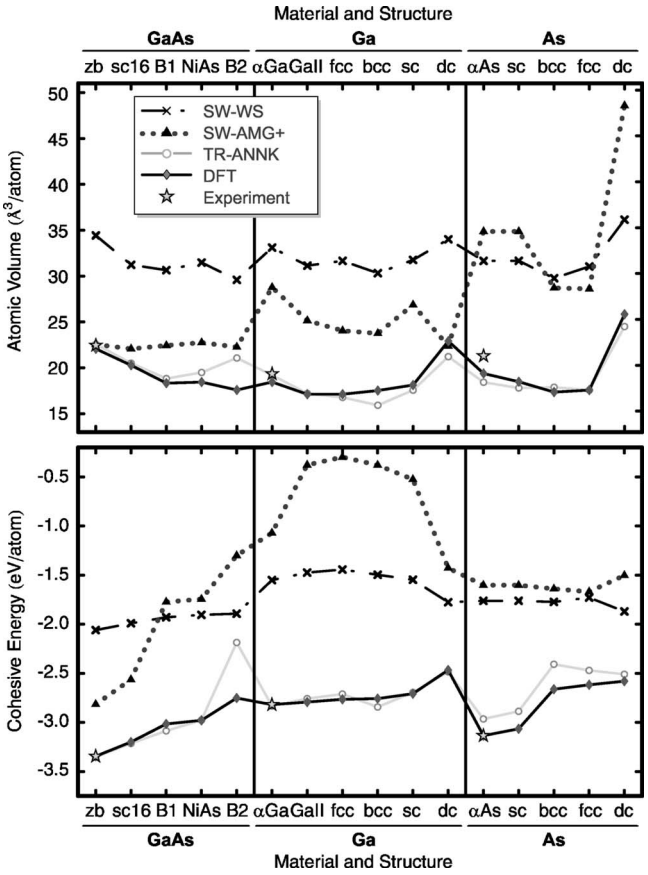

FIG. 1. The (a) atomic volume ($Å^3$/atom) and (b) cohesive energy (eV/atom) predictions for the SW-WS, SW-AMG+, and TR-ANNK potentials are plotted for selected GaAs, gallium, and arsenic phases. Experimental (Refs. 55, 56, 58, 59, and 61) and LDA DFT (Refs. 45 and 65) data are also shown to assess the potentials' predictions.

curate representation of Ga-Ga and As-As interactions. The TR-ANNK potential correctly predicted αAs as the lowest-energy phase for arsenic. The experimentally determined, lowest-energy αGa phase was predicted to be only 0.011 eV/atom less stable than the gallium bcc crystal. Taking into account the many gallium metastable phases that have energies within 0.08 eV/atom of αGa,[45,66,67] the TR-ANNK potential's prediction of gallium crystal stability appears to be reasonable, particularly for an element that is difficult to model.

TABLE I. Bulk elastic modulus data for selected elemental gallium crystal structures. All data have units of GPa. Dashes (—) indicate that no data is available.

	αGa	dc	fcc	sc	bcc
Experiment[a]	61.3	—	—	—	—
DFT[b]	67.4	46.5	65.2	61.3	—
SW-WS	58.7	23.8	175.9	44.8	173.2
SW-AMG+	—	44.1	82.1	74.6	493.5
TR-ANNK	43.4	28.0	1127.9	43.1	55.9

[a]Reference 128.
[b]Reference 45.

TABLE II. Bulk elastic modulus data for selected elemental arsenic crystal structures. All data have units of GPa. Dashes (—) indicate that no data is available.

	αAs	dc	fcc	sc	bcc
Experiment[a]	58.0	—	—	—	—
DFT[b]	58.0	52.6	93.0	96.8	96.8
SW-WS	51.7	26.8	193.4	51.7	195.1
SW-AMG+	92.4	40.5	81.3	92.4	945.0
TR-ANNK	76.5	47.5	87.8	81.1	109.2

[a]Reference 129.
[b]Reference 45.

All three potentials correctly predicted that the lowest-energy phase of GaAs is the zb structure. The SW-WS potential failed to predict the correct cohesive energy and volume for heteropolar GaAs, which limits its usefulness in simulating crystalline GaAs. The GaAs zb phase predicted by the SW-AMG+ potential is anticipated to dominate during MD simulations of GaAs thin film growth because elemental interactions are unduly weak. It is, therefore, concluded that the TR-ANNK potential is likely to be the best choice for modeling atoms where there is a wide range of homopolor and heteropolar coordinated bulk environments.

III. ELASTIC CONSTANTS

During atomic assembly, the incorporation of defects (e.g., arsenic interstitials) or lattice mismatch strains (during heteroepitaxial growth) introduces significant internal stress, which affects the formation of defect structures.[68] Hence, potentials need to predict reasonably precise elastic constants.

The bulk elastic moduli of gallium and arsenic crystal structures calculated by the three potentials have been compared to LDA DFT[45] calculations in Tables I and II. It is evident that the SW-WS potential poorly predicts the elastic constants of all phases of both elements. Closely packed structures (bcc and fcc) were two to three times too stiff, while open structures (dc and sc) were much too soft. The SW-AMG+ parametrization predicted elastic moduli for the dc, fcc, and sc phases, which were all within 25% of LDA DFT data. For arsenic, the αAs and bcc phases were two and

TABLE III. Single crystal elastic stiffness constants for the zb structure of GaAs. Calculations of c_{44} that do not allow internal relaxation are labeled $c_{44}^{(0)}$. All data have units of GPa. Dashes (—) indicate data is not available.

c_{ij}	Expt. (298 K)[a]	DFT[b]	SW-WS	SW-AMG+	TR-ANNK
c_{11}	118.1	123.0	41.9	129.2	124.4
c_{12}	53.2	58.0	21.0	50.3	48.4
c_{44}	59.2	62.0	16.1	55.2	39.1
$c_{44}^{(0)}$	—	75.0	30.3	85.2	73.7

[a]Reference 130.
[b]Reference 131.

eight times stiffer than the DFT calculations. The TR-ANNK potential's bulk elastic moduli were all within 40% of DFT predictions, with the notable exception of the fcc gallium structure, which was much too stiff.

Data for the three independent elastic constants of the GaAs zb structure are shown in Table III. The unrelaxed and relaxed elastic constant data were calculated using molecular statics methods discussed in Appendix B. The SW-WS potential predicted moduli that are much softer than the experimental values or DFT calculations. Clearly, in studies that require deformation or the sampling of environments where atoms reside in highly strained (off-lattice) sites, the SW-WS parametrization is a poor modeling choice because of its inaccurate prediction of elastic constants. Table III shows that the c_{11}, c_{12}, and $c_{44}^{(0)}$ elastic constants determined by the SW-AMG+ and TR-ANNK potentials were quite similar to the DFT predicted and experimentally measured moduli for the GaAs zb phase. However, the relaxed c_{44} elastic constant was predicted most accurately by the SW-AMG+ potential.

IV. POINT DEFECT ENERGETICS

The assembly of GaAs from a vapor on a (001) surface results in the incorporation of point defects, such as antisites, interstitials, and vacancies. The concentration of each point defect type is sensitive to growth conditions, such as temperature, As:Ga flux ratio, and deposition rate.[4,69] The probability that a given defect will form is dependent on the defect formation energy. These defect formation energies can be estimated using the methodology of Zhang and Northrup.[19,70]

The energy of formation of point defects (or defect complexes) can be written for a system of i atom types as

$$\Omega(\mu_e,\mu_i) = E_D + Q_D\mu_e - \sum_i n_i\mu_i, \tag{2}$$

where E_D is the total energy of a supercell containing a defect, Q_D is the charge state of the defect, μ_e is the relative electron chemical potential, n_i is the number of atoms in the defect cell for each atom type i, and μ_i is the corresponding atomic chemical potential for each atom type i. We can omit the charge state term and let $Q_D\mu_e \rightarrow 0$, because the potentials discussed here do not explicitly account for local electronic charge.

Under equilibrium conditions, the sum of chemical potentials for gallium and arsenic atoms in the reservoir equals the bulk chemical potential of the gallium arsenide system, $\mu_{\mathrm{Ga}}+\mu_{\mathrm{As}}=\mu_{\mathrm{GaAs}}^{(\mathrm{bulk})}$. Following Ref. 19, Eq. (2) can be rewritten as

$$\Omega(\mu_e,\Delta\mu) = E_D' - \frac{1}{2}(n_{Ga}-n_{As})\Delta\mu, \tag{3}$$

where

$$E_D' = E_D - \frac{1}{2}(n_{Ga}-n_{As})\mu_{GaAs}^{(bulk)} - \frac{1}{2}(n_{Ga}-n_{As})(\mu_{Ga}^{(bulk)}-\mu_{As}^{(bulk)}) \tag{4}$$

and

TABLE IV. Formation energies (E_D') in eV for simple point defects in GaAs. The defect formation energies were estimated in a periodic computational cell made of 512 atoms.

	Predicted Formation Energy (eV)			
Defect Type	DFT[a]	SW-WS	SW-AMG+	TR-ANNK
Ga vacancy, V_{Ga}	3.15	1.44	2.62	2.16
As vacancy, V_{As}	3.10	1.62	2.69	2.46
Ga antisite, $\mathrm{Ga_{As}}$	2.12	0.47	2.53	1.53
As antisite, $\mathrm{As_{Ga}}$	2.48	0.48	6.00	5.58
Ga interstitial, Ga_i	2.98	2.28	5.69	1.09
As interstitial, As_i	4.07	2.17	10.26	5.91

[a]References 71 and 22.

$$\Delta\mu = (\mu_{Ga}-\mu_{As}) - (\mu_{Ga}^{(bulk)}-\mu_{As}^{(bulk)}). \tag{5}$$

The chemical potential difference, $\Delta\mu$, is limited by the inequalities $\mu_i \leqslant \mu_i^{(bulk)}$ for i atom types gallium and arsenic. These constraints help determine the allowed range of $\Delta\mu$ between $\pm\Delta H_f$. The heat of formation, ΔH_f, for the As $+\mathrm{Ga}\rightarrow\mathrm{GaAs}$ reaction at standard temperature and pressure can be estimated with

$$\Delta H_f = E_{\mathrm{GaAs}}^{(\mathrm{bulk})} - E_{Ga}^{(\mathrm{bulk})} - E_{As}^{(\mathrm{bulk})}, \tag{6}$$

where $E_i^{(\mathrm{bulk})}$ (which is equivalent to $\mu_i^{(\mathrm{bulk})}$ at 0 K) is the cohesive energy of the most stable GaAs, gallium, and arsenic phases. The validity of this approximation is based on the small change in enthalpy between 298 K and 0 K for solid phase gallium, arsenic, and gallium arsenide.

The defect formation energies, $E_D'(\Omega|_{\Delta\mu=0})$, were calculated for gallium and arsenic vacancies (V_{Ga} and V_{As}), both gallium and arsenic interstitials (Ga_i and As_i), and the two antisite defects ($\mathrm{Ga_{As}}$ and $\mathrm{As_{Ga}}$), see Table IV. The samples were first annealed at 800 K for 10 ps and then cooled to 0 K by energy minimization methods. This two-step process allows metastable sites to be avoided. The formation energies calculated here are consistent with those previously determined for Tersoff-based potentials.[71]

DFT defect formation energy calculations[22,71] are also shown in Table IV. The DFT results indicate that the antisite substitutional defects for gallium and arsenic are the most likely to form (under gallium-rich and arsenic-rich environments, respectively). Other point defects, such as the gallium-rich Ga_i or V_{As}, have higher formation energies than the gallium antisite, and, therefore, the concentration of these defects is likely to be less. Moreover, arsenic interstitial point defects would likely have even lower concentrations unless, for example, the environment was extremely arsenic-rich and defects were kinetically trapped.

Although the SW-WS potential predicts defect energies that are unusually small for antisite defects, it correctly predicts that they have the lowest formation energy. In fact, the SW-WS potential predicts the defect formation energy trends better than either of the other two potentials. However, the extremely low formation energies would likely lead to a significant overprediction of defect concentrations.

The SW-AMG+ potential predicts that gallium antisites and gallium vacancies are the most likely defects to form. The SW-AMG+ potential predicted formation energies for the arsenic antisite and interstitial point defects to be anomalously high. Therefore, concentrations of these defects during simulation would likely be much lower than would be expected based on DFT results. Due to its inability to incorporate the excess arsenic into point defects without imposing large energy penalties, SW-AMG+ would not be able to accurately simulate low-temperature growth of GaAs under high arsenic overpressures.[72,73] However, the fact that the gallium antisite has the lowest formation energy does match DFT data well.

The defect formation energies of gallium antisites and interstitials predicted by the Tersoff potential parametrized as TR-ANNK are low. Thus, calculations with this potential are likely to result in erroneously high concentrations of gallium interstitial and antisite defects. In arsenic-rich environments, excess arsenic faces a very large defect formation energy for interstitial and substitutional antisite defects that would reduce the probability of encountering these defects at the levels expected by DFT predictions.

In summary, the SW-WS potential is not a strong choice based on the fact that defect formation energies are extremely low and would likely yield unphysically high concentrations of most point defect types. If the SW-AMG+ potential was used in a stoichiometric or gallium-rich environment, the formation energy magnitudes for gallium-based defects would seem to indicate that this was a reasonable potential choice; however, the potential would likely fail to predict accurate defect concentrations in arsenic-rich environments. The TR-ANNK potential would likely overpredict gallium-based defect concentrations while underpredicting arsenic interstitial concentrations. For a wide range of processing conditions, there is no potential that is clearly superior.

V. MELTING TEMPERATURE

The melting temperature is an indirect measurement of the strength of the interatomic bond (the depth of the interatomic potential well) and the shape of the potential at large interatomic separation excursions. The information reflected in the melting temperature is based on the dynamic sampling of the topology of the bonding energy around each atom. Thus, the predicted melting temperature for a given potential provides an indication of the overall utility of the potential for modeling vapor deposition.

TABLE V. Calculated melting temperatures of GaAs for selected potentials compared with experimental values. Calculations were performed by the equilibrium coexistent phase method introduced by Morris *et al.* (Ref. 74). Dashes (—) indicate that no previous calculations were found in literature.

Potential	T_{melt} (K)	Refs.
Experiment	1513	75
SW-WS	1020±100	—
SW-AMG+	2620±100	—
TR-ANNK	1900±100	45

The melting temperature for each potential was calculated by MD using a method developed by Morris *et al.*[74] in which a half-liquid and half-crystalline supercell is allowed to reach an equilibrium temperature under constant pressure. They showed that the temperature of the two-phase system is then a good approximation to the melting temperature. Using a supercell of 6400 atoms (100 planes with 64 atoms/plane) and a systemwide target pressure of 1 atm, simulations were conducted for 1000 ps of simulated time and are summarized in Table V. The predicted melting temperature values have an uncertainty of ±100 K. The uncertainty range was partially based on pressure oscillations during the calculations and the variation in equilibrium temperatures from repeated runs with different initial conditions.

The melting temperature of GaAs at atmospheric pressure was experimentally determined to be 1513 K.[75] The SW-WS prediction underestimated the experimental melting temperature by 33% but was still reasonably close to the measured value. The SW-AMG+ potential significantly overestimated the phase transition temperature by 73%. The melted crystal and composition profile are shown for a sample calculation of the melting temperature for the TR-ANNK potential, see Fig. 2. Our calculations measured the temperature and pressure of this phase system after 1 ns of simulation time for runs with three different initial average temperatures and found the final temperature to be 1950±150 K and the pressure to oscillate around 1 atm. This value was consistent with the Albe *et al.*[45] estimation of the melting temperature of T_{melt}=1900±100 K. The TR-ANNK potential simulations

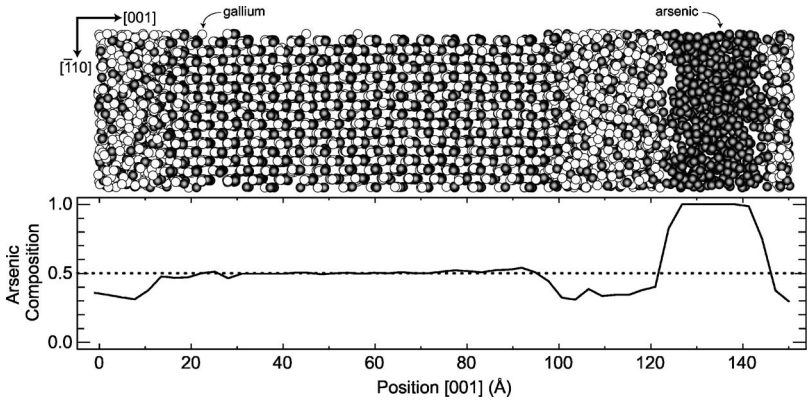

FIG. 2. The GaAs melt at 1904 K in equilibrium, as predicted by TR-ANNK using the method proposed by Morris *et al.* (Ref. 74). The arsenic composition profile clearly identifies the three regions of stoichiometric GaAs, gallium-rich liquid, and pure arsenic liquid.

TABLE VI. Structure, total binding energy (E_B in eV), and average interatomic spacing (r_0 in Å) for As_2 and As_4. Dashes (—) indicate that no data is available.

	Dimer		Tetrahedron		Square	
Source	E_B	r_0	E_B	r_0	E_B	r_0
Experiment[a]	3.96	2.10	10.21	2.44	—	—
DFT[b]	4.05	2.12	10.72	2.46	—	—
SW-WS	0.94	2.86	2.91	3.28	3.51	2.90
SW-AMG+	0.75	3.61	2.74	3.31	2.25	3.18
TR-ANNK	3.96	2.10	9.36	2.44	10.15	2.27

[a]References 77 (dimer) and 78 (tetrahedron).
[b]Reference 79.

resulted in a system consisting of a stoichiometric GaAs solid and a gallium-rich liquid that was separated by a region of pure arsenic liquid.

VI. ARSENIC DIMERS AND TETRAMERS

During the vapor deposition of GaAs thin films, arsenic and gallium are codeposited and assembled on the film surface to form GaAs. The arsenic is in either dimer or tetramer form.[76] The impact dynamics and initial assembly processes are expected to be sensitive to the structure of these incident molecules as well as to that of the surface upon which impact occurs. It is, therefore, important that the structure and bond energies of the free molecules be reasonably approximated by the potentials used for simulations of thin film growth. The molecular binding energy, E_B (i.e., the total energy of isolated atoms minus the total energy of the atoms in the bound state), and the interatomic spacing, r_0, were calculated and compared with experimental data[77,78] and DFT calculations[79] in Table VI.

The dimer and tetrahedral structures and binding energies in Table VI indicate that the As-As bonding interactions in small arsenic clusters are too weak when calculated using the SW-WS and SW-AMG+ parametrizations. This effect was already discussed for crystalline solids and continues as arsenic atoms encounter lower coordinations, see Fig. 1. The TR-ANNK potential, on the other hand, offers a more accurate prediction of As-As bonding, even in arsenic dimers and tetramers. It should be noted that the dimer properties match experimental data exactly for the TR-ANNK potential because of the fitting method employed.[45] Although the bonding energy for As_4 is well predicted by the TR-ANNK potential, the most stable four-atom structure was a planar square structure rather than the experimentally observed tetrahedron arrangement. This occurs because the lowest-energy As-As-As angle is only slightly more than 90°, promoting an arsenic square over the tetrahedron structural form.

Molecular arsenic has very strong bonds, and this directly impacts the mechanism by which the molecules are incorporated into the surface. Therefore, the most accurate vapor deposition simulations with molecular arsenic require that the potentials model these strong molecular bonds well. For the SW parametrizations explored, it is clear that elemental interactions are not well predicted. The strong bonding of arsenic molecules was, however, well predicted by the TR-ANNK potential.

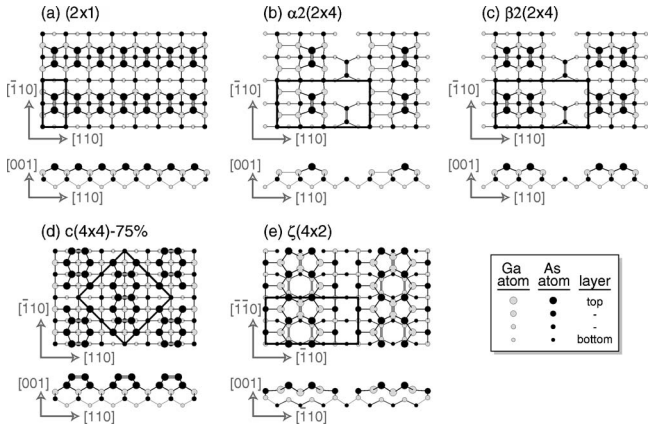

FIG. 3. Top and side projections of GaAs (001) surface reconstructions. Unit cells are marked in black.

VII. SURFACE STRUCTURE ASSESSMENTS

Surface free energy calculations provide a means for determining the dominant surface structure under a range of environmental and surface composition conditions. Accurate predictions of the lowest-energy surface structure are essential for high fidelity estimates of the energy barriers and the incorporation paths encountered by gallium or arsenic during atomic assembly on either arsenic-rich or gallium-rich surfaces.

The GaAs (001) surface structure has been extensively studied by numerous experimental and computational methods.[80–83] Figure 3 shows selected surface reconstructions that are important to subsequent discussions. The generally accepted surface reconstructions for the (001) surface are the arsenic-terminated $\beta 2(2\times 4)$ [Fig. 3(c)],[84–86] the arsenic-terminated $\alpha 2(2\times 4)$ [Fig. 3(b)],[87] the arsenic-rich $c(4\times 4)$[88] [Fig. 3(d)], and the gallium-rich $\zeta(4\times 2)$[18] [Fig. 3(e)], reconstructions. The presence of these surface reconstructions depends on the surface temperature and the pressure and composition of the vapor (As:Ga flux ratio).[89]

Provided that the surface is in equilibrium with the vapor, a simple thermodynamic analysis can be used to calculate changes in the total free energy as arsenic and gallium atoms are interchanged between a bulk material (thermodynamic reservoir) and an atmospheric vapor (atom reservoir) at the surface.[90,91] Stable surfaces are predicted by minimizing the surface free energy per unit area with respect to surface composition and geometry. When in thermodynamic equilibrium with its vapor, the surface free energy can be written as a function of the relative arsenic chemical potential ($\mu_{As}-\mu_{As}^{(bulk)}$), which ranges between 0 and ΔH_f.[91] This range effectively limits the formation of pure arsenic or gallium on the GaAs (001) surface in the presence of both arsenic and gallium sources at equilibrium.[90]

Using this technique, Lee *et al.* predicted the surface free energies of different surface reconstructions[18] with GGA

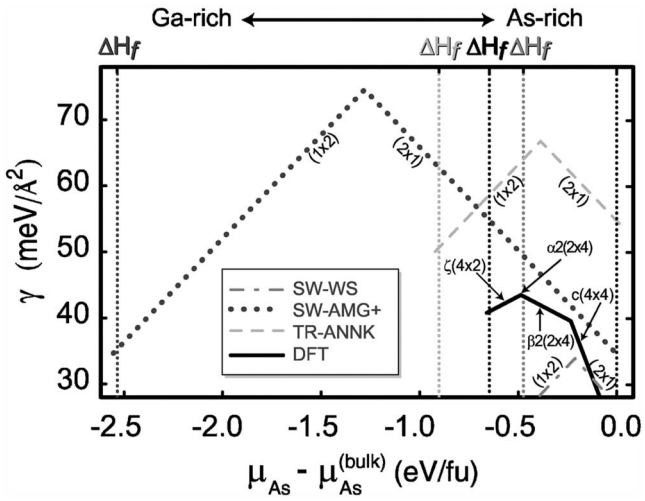

FIG. 4. The surface free energy (γ) for low-energy GaAs (001) surface reconstructions plotted versus the arsenic chemical potential. DFT data (Ref. 18) is compared to the predictions of the SW-WS, SW-AMG+, and TR-ANNK potentials. The GaAs heat of formation, ΔH_f, is shown in the upper horizontal axis for the DFT model and each interatomic potential. Experiments report $\Delta H_f = -0.74$ eV/fu (Ref. 58).

DFT, see Fig. 4. A similar approach can be used to determine the predicted surface energies of the various reconstructions using interatomic potentials, also shown in Fig. 4. The total energy of a computational supercell for each reconstructed surface was determined using a slab of 1500–1700 atoms (25–27 layers with 64 atoms/layer measuring 32 Å $\times$ 32 Å) with an identical top and bottom surface. The central plane was fixed and the entire system was then relaxed using energy minimization (see Appendix B). The surface area, bulk cohesive energies, and the number of atoms on each surface were then used to calculate the surface free energy.[17,91]

All three potentials predict stable (1×2) gallium-rich and (2×1) arsenic-rich surfaces. These structures are composed of simple dimer rows instead of the (2×4) family of surface reconstructions with missing dimers seen in DFT calculations, see Figs. 3(a)–3(c). DFT predicted that the lowest-energy surface reconstructions are the $\zeta(4\times2)$, $\alpha2(2\times4)$, $\beta2(2\times4)$, and $c(4\times4)$ as one moves from a gallium-rich to arsenic-rich surface condition (Fig. 4). All of the DFT-predicted, low-energy surfaces have been experimentally observed on GaAs (001) surfaces.[80–83,87] These lowest-energy surface reconstructions on the GaAs (001) surface were clearly not obtained using any of the three interatomic potentials. The poor agreement between the interatomic potential and DFT predictions is understandable since (001) surfaces are polar and electrons are not explicitly addressed by any of the potentials.[92–94]

The inability of any of the potentials to account for the complexities of GaAs (001) surfaces will clearly limit the fidelity of some MD studies of thin film growth. For example, the topology of the surface energy profile will be significantly altered when the extra trenches of the $\beta2(2\times4)$ surfaces [Fig. 3(c)] are not present in a simulation. The resulting energy barriers and transition pathways for gallium or arsenic diffusion on arsenic-rich and gallium-rich surfaces are then likely to be inaccurately represented. This may be especially critical for simulations of high-temperature, low-deposition rate thin film growth, where surface kinetics are sufficiently rapid that complex surface reconstructions can occur during deposition. Simulations at lower temperatures where the atom mobility is significantly lower may be less affected since the slower kinetics can impede the reorganization of the surface structure.

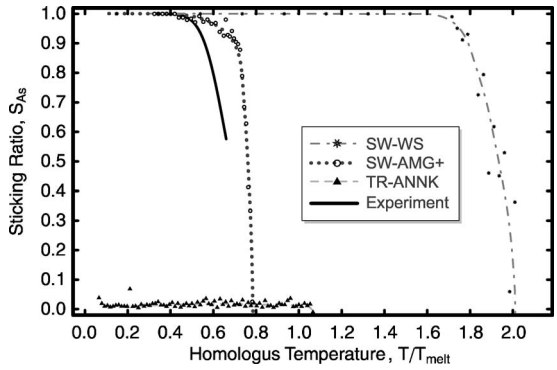

FIG. 5. Arsenic dimer sticking fraction, S_{As}, on a gallium-rich surface is calculated for the three potentials (SW-WS, SW-AMG+, and TR-ANNK) and is compared with an empirically fit expression (solid black line). Simulated homologous temperatures are used to equate temperatures for each potential.

VIII. STICKING RATIO DURING ARSENIC DIMER VAPOR DEPOSITION

Further insights into the utility of current interatomic potentials for simulating the vapor deposition of GaAs can be gained by investigating the sticking of As_2 on the low-energy gallium-rich GaAs (001) surface. During molecular beam epitaxy, gallium has been found to have nearly 100% sticking probability for surface temperatures below 915 K.[73] The sticking ratio of As_2, however, is highly sensitive to surface temperature and surface composition. The arsenic dimer sticking probability on both gallium-terminated and arsenic-terminated GaAs (001) surfaces has been found to be quite high for deposition temperatures between 650 K and 750 K.[15,95–97] However, as the surface temperature increases, the sticking probability rapidly decreases.

An arsenic sticking ratio, S_{As}, can be defined as the number of arsenic atoms that stick to the surface divided by the number of atoms that impact the surface from an incident As_2 flux ($0 \leqslant S_{As} \leqslant 1$). Tok *et al.* collected experimental sticking probability data on a gallium-rich (4×2) surface reconstruction where Ga-As dissociation was assumed to be negligible.[73] Their sticking probability data for three fluxes were fitted to an Arrhenius expression (with an activation energy of 0.91 eV) between 673 K and 853 K and is plotted as the solid black line in Fig. 5.

The As_2 sticking ratio predictions for the three potentials were calculated using MD simulations, see Fig. 5. These MD simulations utilized a nine-layer substrate with the bottom two layers fixed. Four middle layers were under temperature

control to maintain a constant substrate temperature,[98] and the top three layers were thermally unconstrained. The computational cell had in-plane periodic boundary conditions. The in-plane dimensions of the cell were 16 Å × 16 Å. The top (001) (1 × 2) surface was gallium-terminated. An arsenic dimer was deposited 100–500 times on an identical (fresh) surface at random atom positions normal to the (1 × 2) gallium-rich (001) surface. Deposited dimers were given an initial translational energy of 0.1 eV/atom. An average kinetic energy of 0.1 eV/atom is comparable to a temperature of 1160 K, which is reasonably close to the evaporation cell temperature of gallium.[76]

Desorption events were monitored for up to 100 ps following the initial impact. The sticking probability was then determined and the series of simulations repeated for simulation temperatures, T, between 300 K and 1500 K at temperature steps of 25–100 K. The corresponding homologous temperature, T/T_{melt}, was obtained using the potential's predicted GaAs melting temperature (Table V). The average sticking ratio, S_{As}, for each potential is plotted against the homologous temperature in Fig. 5.

Evaporation was observed to begin at ~147% T_{melt} for the SW-WS potential and ~69% T_{melt} for the SW-AMG+ potential. The arsenic dimer sticking ratio predicted by the SW parametrizations was nearly constant below the evaporation temperature, T_{evap}. At low temperatures, the vast majority of all arsenic dimers were incorporated into the (001) surface. This agrees well with the experimental data at low temperatures where near unity sticking probability is both predicted and experimentally observed.

The TR-ANNK potential incorrectly predicts significant As_2 desorption over the entire temperature range. In fact, internal molecular energies and translation energies of 0.5 eV were required to produce a sticking ratio of 6% at a scaled equivalent temperature of 300 K, shown in Fig. 5. The case of 0.1 eV of translational energy with no internal dimer energy (as was the case for the two SW parametrizations) predicted a sticking ratio below 0.1%. Experimentally, significant As_2 desorption occurs at temperatures only above 800 K;[76] however, the TR-ANNK potential underestimates the As_2 binding energy over most of the temperature range.

The dynamic study of the bonding of arsenic dimers on gallium-rich surfaces separates the three potentials into two categories. The first group is defined by the two SW parametrizations, which predict strong As_2/gallium-terminated (1 × 2) surface bonding that does not break until the temperature approaches the melting temperature. The TR-ANNK parametrization of the Tersoff potential falls into the second category, where As_2/gallium-rich (1 × 2) surface bonding is weak and desorption is the dominant process. These dramatic differences in the bonding of As_2 to gallium-rich (001) surfaces cannot be understood only from bulk property predictions, yet surface bonding must be understood for the accurate simulation of vapor deposition.

IX. DISCUSSION

A large body of literature has been produced to simulate GaAs using classical interatomic potentials. From these potentials (Appendix A), three potentials (SW-WS,[37] SW-AMG+,[38,39] TR-ANNK[45]) have been evaluated in detail for their ability to predict bulk, arsenic vapor, and surface properties. Atomic volumes, cohesive energies, and elastic properties of GaAs were used to quickly assess the strengths and weaknesses of each potential for coordinated environments between 4 and 12. The study of arsenic clusters and (001) surfaces helped explore each potential's response to lower coordinated environments.

The SW parametrizations studied do not predict the complexities of bonding environments when they significantly deviate from tetrahedral or, in the case of a weak angular term, close-packed fcc structures (as was the case for arsenic interactions of SW-WS). The SW-WS potential predicted weak bonding and elastic constants for all structures and should likely be avoided. The SW-AMG+ predicted reasonably good bulk and elastic properties for the zb structure, but elemental properties were poorly predicted. The sticking ratio trend of As_2 to the (001) gallium-rich surface as a function of temperature was similar to the measured experimental values.

The Tersoff potential, as parametrized by Albe *et al.*, predicts a much larger assortment of crystalline bonding and structures than do either of the SW parametrizations. TR-ANNK also allows desorption, which is very useful in studying surface interfaces at extremely high temperatures. However, desorption was overpredicted due to the extremely weak molecular arsenic/(001) surface bonding, as demonstrated in the sticking ratio calculations. (It is possible that this potential could be used for atomic arsenic deposition studies.[99])

The SW parametrizations were shown to predict high As_2 sticking probabilities, while the Tersoff parametrization predicted a low estimate with significant As_2 desorption over the entire temperature range, when the simulation data were compared to experimental data. These dramatic differences in surface bonding of As_2 to gallium-rich (001) surface reconstructions predicted by the potentials cannot be captured by simply checking the bulk properties used to develop the parameters. Therefore, surface bonding interactions should be tested before current and future potential parametrizations are utilized.

All potentials studied were shown to incorrectly predict the simple dimer row surfaces as the most stable (001) surface reconstructions over the more complex structures seen in experiments and as predicted in DFT calculations. This effect is especially critical for high-temperature vapor deposition, where surfaces can quickly respond to atmospheric and temperature conditions to form a variety of complex surface reconstructions. Lower temperatures decrease the atom mobility and reconstruct less dramatically; nevertheless, accurate surface bonding is important to modeling vapor deposition simulations.

The ability of each potential format to represent salient physics for bulk, surface, and molecular bonding directly impacts its ability to model the GaAs system. The major deficiencies with each potential can be generally related back to an absence of physics in the model format. The SW (Ref. 47) and Tersoff[45,49,53] potential formats represent two approaches to capturing the physics of bonding. The SW for-

mat involves an empirical combination of two-body energy terms (ϕ) and a three-body angular term ($\cos\theta+1/3$),[47]

$$E_{\mathrm{SW}} = \frac{1}{2}\sum_i \sum_{j\neq i}\left[\phi_{R,ij} - \phi_{A,ij} + \sum_{k(\neq i,j)} \phi_{B,ij}\phi_{B,jk}\left(\cos\theta_{jik} + \frac{1}{3}\right)^2\right]. \quad (7)$$

The first term, $\phi_{R,ij}$, is a two-body pair function that approximates the increase in energy produced by the overlap of valence and core electron shells of the bonding atoms (i and j) due to the Pauli exclusion principle and an electron Coulomb repulsion.[100,101] The attractive two-body energy, $\phi_{A,ij}$, and the three-body term serve to stabilize the open structure phases for the SW approximation. For the GaAs system, the bonding type includes *sp*-valent (metallic and covalent) bonding. In general, the spherically symmetric two-body attractive terms can accurately predict van der Waals forces.[101] Angular dependent covalent bonding is approximated with the three-body angular term (centered around atom i and involving the vectors $\vec{ij}$ and $\vec{ik}$ to atoms j and k) and a pairwise function, ϕ_B. This three-body term provides a positive energy for any structure that does not have the prescribed equilibrium angle. Stillinger and Weber fixed this at $\arccos 1/3 = 109.47°$ (the tetrahedral bond angle).[47] The angular term also defines how the energy behaves as the tetrahedral bonds are distorted. In principle, the equilibrium angle could be changed to accommodate other structures;[102] however, most phases have more than one angle, which may make the SW approach less applicable to these more complex structures.

Silicon[47] and germanium[103] parametrizations of the SW format have proven useful in modeling vapor deposition on the (001) surface.[104–108] These material systems strongly favor tetrahedral bond angles and thus this approximation is adequate—although the bond angles have been reported to be too stiff when compared to tight binding theory calculations.[109] Furthermore, the simplicity of the SW potential makes fitting the free parameters a straightforward task for a tetrahedral solid, because the independent free parameters can be determined by fitting the lattice parameter, cohesive energy, and three elastic constants. In such a manner, the low-energy GaAs zb structure, stability, and elastic constants were effectively captured in the SW-AMG+ parametrization. However, As-As and Ga-Ga interactions are more complex in their bonding preferences, and the SW approximation becomes less effective in such elemental environments, as was demonstrated in previous sections.

Upon inspection of Eq. (7), it stands to reason that the lowest-energy phases that can be predicted by this format for nearest-neighbor systems have either tetrahedral (if the three-body term is strong) or close-packed (if the three-body term is quite weak) structures. The two examples of SW parametrizations shown above follow these trends. Clearly if a more accurate potential is required for elements and alloys not in column IV, a more transferable model must be used; however, if a simple model is needed to simulate single phase dynamics, then the SW approach can be quite useful.

Like the SW potential, the Tersoff potential is also based on repulsive (ϕ_R) and attractive (ϕ_A) two-body terms, but also includes a term sensitive to the bonding environment, $\bar{B}$, which multiplies the attractive pairwise energy term, $\phi_{A,ij}$,[49,52]

$$E_{\mathrm{TR}} = \frac{1}{2}\sum_i \sum_{j\neq i}(\phi_{R,ij} - \bar{B}_{ij}\phi_{A,ij}). \quad (8)$$

This concept was originally proposed by Abell[110] and can be an effective way of capturing a wide range of structural properties within a simple format.

The format of the many-body term as empirically expressed by Brenner[53] can be related to the analytical second moment term of the bond-order potential (BOP) derived from tight binding theory by Pettifor *et al.* for covalent systems with half-full *sp*-valence shells.[111] The second moment bond-order term, Θ_{ij}, for BOP takes the general form of

$$\Theta_{ij} = \left(1 + \frac{\Phi_{ij} + \Phi_{ji}}{2}\right)^{-1/2}, \quad (9)$$

while the empirical Tersoff bonding term takes the following form,

$$\bar{B}_{ij} = \frac{1}{2}[(1+\chi_{ij})^{-1/2} + (1+\chi_{ji})^{-1/2}]. \quad (10)$$

The BOP derivation was done based on the bond-centered perspective; however, an atom-centered form can also be used,[112] which can yield a many-body format that more closely approximates the Tersoff term as expressed by Brenner.[49,53] Assuming $\Phi \approx \chi$, then equivalence of the simplified BOP and Tersoff formats can be established. Based on the similarity of the empirical Tersoff format to the derived BOP covalent σ bond format, it is plausible that the Tersoff format approximates σ bonding to the level of the two self-returning hops, which are equivalent to approximating the second moment of the density of states, i.e., the mean square width.[111] Additional sampling of the local environment based on derivations by Pettifor and Oleinik may prove useful for better approximations of metallic and the primary (σ) and secondary (π) covalent bonding for *sp*-valent materials.[113] This may especially be true for arsenic, which is strongly dependent on π bonding.[114,115] The inclusion of four-body angles (included in the π bond order) might also help predict higher stacking fault energies, which are likely to be very small in their absence.[116] Another suggestion to help improve the Tersoff format's prediction of defect formation energies and molecular and/or surface bonding properties would be to expand the atom-type dependence of the angular parameters from only i and k atom types to all the i, j, and k atom types.

The work above clearly shows that the Tersoff potential successfully predicted a large number of bulk structures when parametrized by Albe *et al.*[45] However this transferability requires careful parametrization. For example, the TR-ANNK parametrization had a previously unreported low-energy bcc gallium phase. Therefore, when fitting Tersoff or BOP model parameters, a large number of structures should be rigorously evaluated due to the flexibility of this format.

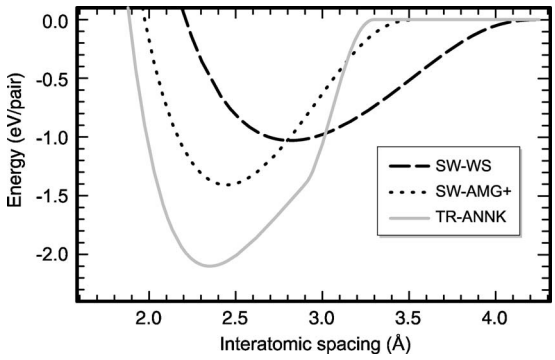

FIG. 6. The energy curves for GaAs dimers for the SW-WS, SW-AMG+, and TR-ANNK potential parametrizations.

Furthermore, care should be taken to not force a fit to a particular format that does not capture the physics of the bonding (e.g., arsenic bonding without the secondary covalent π bonding).

While the choice of the functional form of the two-body terms and its cutoff is quite flexible, a few general guidelines can be gleaned from the parametrizations discussed in this paper. To illustrate this point, the pair potential energy wells ($\bar{B}=1$ for Tersoff and $\phi_B=0$ for SW) are shown in Fig. 6. The Tersoff functional form[49] has a strong trigonometric cutoff term that can be used to bring the two-body functions quickly to zero. As can be seen in Fig. 6, the energy versus interatomic spacing curve predicted by the TR-ANNK parametrization has a more abrupt change in slope than either of the SW potential parametrizations. Such sharp changes in slope can cause difficulties in the numerical calculation of energies and forces in simulations that sample this tail of the energy curve frequently. In response, a smaller time step must be used, which makes simulation less time efficient. We have found that short cutoffs also play a part in increasing the quantity of metastable surface sites. The use of a short cutoff can also be the product of an attempt to force a format to capture desired bulk properties—this should be avoided. The SW potentials have had reasonably good success in modeling melted systems;[47] the use of longer-range, smoother cutoffs may play a part in this success.

Lastly, in an attempt to address the incorrect surface reconstruction of phases demonstrated by both the SW and the Tersoff potentials, one might pursue an explicit electron accounting scheme. Such a model is empirically quantified by the electron counting rule.[93,94] In this scheme, the total number of electrons donated by each atom is required to match the number of electrons in each covalent bond. This requirement disallows the (1×2) and (2×1) dimer-row surface reconstructions that were dominant for all the potentials discussed previously.[117] If an effective means for converting this rule into an energy was developed during MD simulation, then it stands to reason that a more accurate surface free energy diagram could be constructed.

X. CONCLUSIONS

(1) The Stillinger-Weber (SW) potentials parametrized respectively by Wang and Stroud[37] (SW-WS) and by Angelo and Mills and Grein *et al.*[38,39] (SW-AMG+) and a Tersoff function parametrized by Albe *et al.*[45] (TR-ANNK) have been evaluated for their suitability for simulating thin films in the GaAs system. The elemental and binary bulk properties predicted by these three potentials have been evaluated. Closest agreement with experimental and *ab initio* results were obtained with the TR-ANNK potential. The SW-WS potential was unable to reproduce energies, volumes, and elastic constants consistent with experimental and *ab initio* values. Simulations involving homopolar bonding were poorly predicted by both the SW-WS and SW-AMG+ potentials. Defect properties were best predicted by the SW-AMG+ potential (under limited environmental conditions); however, none of the potential parametrizations performed well in this regard.

(2) The complexities of the GaAs (001) surface reconstruction were not captured by any of the interatomic potentials. Further work is needed to develop potentials that introduce the physics responsible for the appearance of dimer trenches on the $\beta2(2\times4)$ and $\zeta(4\times2)$ reconstructions on the (001) surfaces of GaAs.

(3) The temperature dependence of arsenic dimer sticking probability was evaluated. Homologous temperatures were defined to relate experimental and predicted temperatures. Simulations of arsenic dimer deposition onto gallium-rich GaAs (001) surfaces indicated that the SW potential parametrizations predict near 100% sticking probability. This is experimentally valid at temperatures below $\sim$800 K.[76] The TR-ANNK potential predicts a high rate of desorption, so much so that it cannot be used to simulate vapor deposition with molecular arsenic.

(4) Due to its difficulty with bulk properties, the SW-WS potential should be avoided and the SW-AMG+ potential used in its place. The use of the SW-AMG+ potential should be limited to Ga-As interactions because elemental interactions were poorly modeled. Thus, the SW-AMG+ parametrization might be useful for stoichiometric GaAs thin film growth under equiatomic flux conditions. The TR-ANNK potential had great success in many areas; however, (001) surface/molecular bonding was poorly captured. Therefore, the TR-ANNK parametrization may best perform in atomic flux growth conditions. Nevertheless, there is much room for improvement in the modeling of GaAs properties and care should be taken in applying these and other interatomic potentials to vapor deposition studies.

ACKNOWLEDGMENTS

We are grateful for helpful discussions of this work with David Pettifor, Ralf Drautz, Leonid Zhigilei, Brian Gillespie, and Stuart Wolf. This study was supported by DARPA/ONR, Contract No. N00014-03-C-0288, under the direction of Dr. C. Schwartz and Dr. J. Christodoulou.

APPENDIX A: POTENTIAL ENERGY FUNCTION SUMMARY

Several competing interatomic potential energy formats have been proposed for the covalent system.

TABLE VII. The potential energy functions and parametrizations developed for GaAs are evaluated based on three simple criteria: (1) continuity of energy and force functions, (2) the GaAs zb phase must have a negative heat of formation and is required to be the lowest-energy binary phase, and (3) GaAs zb mechanical stability ("×" denotes a failure, "√" indicates a success, and "—" indicates that the measurement has not been made). Information for the IKD, IKD-mod, and CS potentials and the TR-Smith, TR-SJWC, and TR-SJWC0 potentials' surface properties were gathered from literature.

	Assessment Criterion			
Potential	1	2	3	Refs.
LJ-AT	√	√	×	36 and 132
SW-WS	√	√	√	37
SW-AM	√	×	√	38
SW-AMG+	√	√	√	38 and 39
IKD	×[a]	—	—	40
IKD-mod	×[a]	—	—	121 and 122
CS	√	×	√	41 and 123
TR-Smith	×	√	√	42, 123, and 133
TR-SJWC	×	√	√	43, 123, and 133
TR-SJWC0	×	√	√	123, 124, and 133
TR-ANNK	√	√	√	45

[a]The IKD potentials would pass this criteria if a single equilibrium angle was to be chosen.

Lennard-Jones-Axilrod-Teller[118] (LJ-AT), Stillinger-Weber[46,47] (SW), Ito-Khor-Das Sarma[40,119] (IKD), Conrad-Scheerschmidt[41] (CS), and Tersoff[44,49,52,53] (TR) potential formats have been proposed for multicomponent covalent systems. A brief analysis of three characteristics that strongly influence the ability to perform molecular dynamics (MD) simulations are summarized for the GaAs parametrizations of these potentials. Potentials and parametrizations that meet these criteria are noted and discussed in greater detail in the body of this paper.

The first requirement is a consequence of the large atomic displacements from the ideal crystal or surface lattice positions encountered in vapor deposition simulations. This therefore requires the potential energy function, the first derivative (interatomic forces) step, and the second derivative (elastic constants) to be continuous (C^2). A second criterion can be identified from thermodynamic considerations. The formation of a GaAs zinc blende (zb) phase structure from elemental gallium and arsenic must be an exothermic process.[58] Additionally, the zb phase is required to be the most stable GaAs phase. A third criterion requires that solids must possess mechanical stability, which can be calculated from the predicted elastic constants. The cubic GaAs zb phase has three independent elastic constants, c_{11}, c_{12}, and c_{44}. Two of the elastic constants can be combined to give the bulk modulus, $B=(c_{11}+2c_{12})/3$, and the shear modulus, $c'=(c_{11}-c_{12})/2$. Mechanical stability for cubic crystals then requires that B, c', and c_{44} must all be positive.[120]

Table VII summarizes the performance of 11 potentials with regard to the criteria described above. The LJ-AT parametrization by Choi *et al.*[36] has a continuous functional form; however, from our calculations, it appears that $c_{44}<0$. Thus, the second criteria failed. The multielement extension of the widely used SW potential was parametrized by Wang and Stroud[37] (SW-WS), Angelo and Mills[38] (SW-AM), and a revised parametrization by Grein *et al.*[39] (SW-AMG+). The SW-WS and SW-AMG+ potential parametrizations were analyzed in this paper; however, SW-AM was omitted because the parameters defining the Ga-Ga and As-As interactions were set equal to those of the Ga-As interaction (i.e., $\Delta H_f=0.0$ eV/fu, second criteria). Unfortunately, the IKD parametrization[40] and the format extension (IKD-mod)[121,122] could not be used for MD applications, because the equilibrium angle in the many-body term had no continuous analytical expression (first criteria).[41,42] (If instead a fixed equilibrium angle was used, the potential would then be C^2; however, it would not be transferable across the structures in the same way it was originally published.) The CS parametrization[41] was not used because an inaccurate low-energy GaAs phase was found (second criteria) during melting and recrystallization.[123] The Tersoff potential format was parametrized in succession by Smith[42] (TR-Smith), GaAs interactions were revised by Sayed *et al.* (TR-SJWC) to improve elastic constants,[43] and then a small change to the TR-SJWC parametrization was suggested[123,124] (TR-SJWC0). All of the Tersoff parametrizations discussed so far are based on Smith's elemental parametrizations of gallium and arsenic (TR-Smith, TR-SJWC, TR-SJWC0). The arsenic parameter set ($n<1$ in the multibody term) causes the force to become infinite for the arsenic dimer. Thus, the functional form is discontinuous (first criteria) and cannot be used in MD simulations. Another parametrization by Albe *et al.*[45] (TR-ANNK) was more recently suggested with a slightly revised format.[53] Of these parametrizations, the SW-WS (Ref. 37), SW-AMG+ (Refs. 38 and 39), and TR-ANNK (Ref. 45) parametrizations were studied.

APPENDIX B: MOLECULAR STATICS

Molecular statics methods are used to calculate material properties without the influence of kinetic energy. Material properties estimated in this environment are cohesive energy, atomic volume, and elastic constants of bulk phases; dimer and tetramer cluster energies and structures; and the surface energy of (001) surface reconstructions. The calculation of each of these properties requires that atoms in the computational cell be moved until the system energy is minimized. This motion can involve the group movement of atoms (as is done for highly symmetric crystalline phases) or may optimize individual atom positions (as is the case for surface relaxation).

The calculations for energy, lattice structure, and elastic constants were performed in the symbolic computing environment of MATHEMATICA.[125] Each potential energy function was implemented as an analytic function of the spacing and angles between atoms. The potential energy was then determined as a function of lattice parameters for bulk crystals and atom positions for small clusters. These cohesive and binding energies can then be minimized with respect to lat-

tice parameters and atom positions to find the lowest-energy crystal and cluster structures.

The method of energy minimization used by MATHEMATICA[125] is a combination of the conjugate gradient method and Levenberg-Marquardt algorithms.[126] The minimization scheme for crystals varies the lattice parameters and not the atomic positions, which allows properties for metastable phases to be easily determined. The optimized crystal parameters can then be used to calculate the atomic volume from the lattice vectors defining the unit cell. The crystal unit cells not already in orthogonal form (e.g., αAs and αGa) were transformed into larger cells so that an orthogonal crystal definition can be used.

The minimization of potential energy for clusters allowed interatomic spacing and angles to be optimized. The minimum dimer energy and interatomic spacing can be determined analytically. The lowest-energy tetramer structure was determined by the relaxation[125] of six different starting structures of either the chain, zig-zag chain, square, rhombus, **Y**, or tetrahedron configurations.

The bulk modulus was calculated for each crystal, while the c_{11}, c_{12}, and c_{44} shear elastic constants were determined for the GaAs zinc blende (zb) crystal. The second-order elastic response to deformation was calculated without regard to internal atom relaxation and thus is an estimate of the observed elastic response. These were calculated analytically and numerically in MATHEMATICA using the minimized energy lattice parameters. The bulk modulus was calculated analytically with $B=\Omega\delta^2U/\delta\Omega^2$, where Ω is the atomic volume. The elastic constants for GaAs zb were numerically calculated. The vectors between atoms were strained with a strain matrix in Voigt notation.[127] The unrelaxed elastic constants were then calculated from

$$c_{ij}^{(0)} = \frac{1}{\Omega}\frac{\delta^2 U}{\delta\epsilon_i\delta\epsilon_j}\bigg|_{\epsilon_i=\epsilon_j=0}, \tag{B1}$$

where U is the potential energy for the given format and the superscript (0) indicates that the internal positions were not relaxed.

The relaxed elastic constant (c_{44}) was calculated at a series of strains using molecular statics methods as implemented in the FORTRAN code with the conjugate gradient energy minimization method.[126] Internal atom positions were allowed to relax within the strain field. The curvature of the energy versus strain curve was then analyzed and c_{44} was calculated from Eq. (B1).

Free surfaces were also calculated within the conjugate gradient method implemented in a FORTRAN code, which has a significantly faster computational cycle than MATHEMATICA. An entire system of 1500–1700 atoms was relaxed with respect to both individual atomic lattice coordinates and lattice parameters.

*Author to whom correspondence should be addressed. Email address: murdick@mailaps.org

[1] P. K. Bhattacharya, in *Properties of Gallium Arsenide*, 3rd ed., edited by M. R. Brozel and G. E. Stillman (INSPEC, London, 1996), Vol. 16, pp. 861–873.
[2] M. Feng, P. J. Apostolakis, and W-H. Chang, in *Properties of Gallium Arsenide*, 3rd ed., edited by M. R. Brozel and G. E. Stillman (INSPEC, London, 1996), Vol. 16, pp. 785–798.
[3] H. Ohno, Science **281**, 951 (1998).
[4] J. I. Landman, C. G. Morgan, J. T. Schick, P. Papoulias, and A. Kumar, Phys. Rev. B **55**, 15581 (1997).
[5] R. Kaspi, in *Properties of Gallium Arsenide*, 3rd ed., edited by M. R. Brozel and G. E. Stillman (INSPEC, London, 1996), Vol. 16, pp. 601–607.
[6] K. Mahalingam, N. Otsuka, M. R. Melloch, J. M. Woodall, and A. C. Warren, J. Vac. Sci. Technol. B **9**, 2328 (1991).
[7] J. Villain, J. Phys. I **1**, 19 (1991).
[8] D. D. Vvedensky, Comput. Mater. Sci. **6**, 182 (1996).
[9] M. F. Gyure, C. Ratsch, B. Merriman, R. E. Caflisch, S. Osher, J. J. Zinck, and D. D. Vvedensky, Phys. Rev. E **58**, R6927 (1998).
[10] C. Ratsch, M. F. Gyure, R. E. Caflisch, F. Gibou, M. Petersen, M. Kang, J. Garcia, and D. D. Vvedensky, Phys. Rev. B **65**, 195403 (2002).
[11] M. Itoh, G. R. Bell, A. R. Avery, T. S. Jones, B. A. Joyce, and D. D. Vvedensky, Phys. Rev. Lett. **81**, 633 (1998).
[12] B. A. Joyce, D. D. Vvedensky, G. R. Bell, J. G. Belk, M. Itoh, and T. S. Jones, Mater. Sci. Eng., B **67**, 7 (1999).
[13] D. D. Vvedensky, M. Itoh, G. R. Bell, T. S. Jones, and B. A. Joyce, J. Cryst. Growth **201**, 56 (1999).
[14] G. R. Bell, M. Itoh, T. S. Jones, B. A. Joyce, and D. D. Vvedensky, Surf. Sci. **433**, 455 (1999).
[15] M. Itoh, J. Pediatr. (St. Louis) **66**, 53 (2001).
[16] A. A. Demkov, O. F. Sankey, J. Gryko, and P. F. McMillan, Phys. Rev. B **55**, 6904 (1997).
[17] N. Moll, A. Kley, E. Pehlke, and M. Scheffler, Phys. Rev. B **54**, 8844 (1996).
[18] S-H. Lee, W. Moritz, and M. Scheffler, Phys. Rev. Lett. **85**, 3890 (2000).
[19] J. E. Northrup and S. B. Zhang, Phys. Rev. B **47**, R6791 (1993).
[20] S. Pöykkö, M. J. Puska, and R. M. Nieminen, Phys. Rev. B **53**, 3813 (1996).
[21] C. G. Morgan, P. Kratzer, and M. Scheffler, Phys. Rev. Lett. **82**, 4886 (1999).
[22] G. Zollo and R. M. Nieminen, J. Phys.: Condens. Matter **15**, 843 (2003).
[23] G. Zollo, Y. J. Lee, and R. M. Nieminen, J. Phys.: Condens. Matter **16**, 8991 (2004a).
[24] P. Kratzer and M. Scheffler, Comput. Sci. Eng. **3**, 16 (2001).
[25] P. Kratzer and M. Scheffler, Phys. Rev. Lett. **88**, 036102 (2002).
[26] P. Kratzer, E. Penev, and M. Scheffler, Appl. Phys. A: Mater. Sci. Process. **75**, 79 (2002).
[27] P. Kratzer, E. Penev, and M. Scheffler, Appl. Surf. Sci. **216**, 436 (2003).
[28] A. Nordsieck, Math. Comput. **16**, 22 (1962).
[29] M. E. Bachlechner, A. Omeltchenko, A. Nakano, R. K. Kalia, P. Vashishta, I. Ebbsjö, and A. Madhukar, Phys. Rev. Lett. **84**, 322

(2000).
[30] X. Su, R. K. Kalia, A. Nakano, P. Vashishta, and A. Madhukar, Appl. Phys. Lett. **78**, 3717 (2001).
[31] M. S. Daw and M. I. Baskes, Phys. Rev. B **29**, 6443 (1984).
[32] M. S. Daw, Phys. Rev. B **39**, 7441 (1989).
[33] R. A. Johnson, Phys. Rev. B **39**, 12554 (1989).
[34] H. N. G. Wadley, X. Zhou, R. A. Johnson, and M. Neurock, Prog. Mater. Sci. **46**, 329 (2001).
[35] X. W. Zhou, H. N. G. Wadley, J-S. Filhol, and M. N. Neurock, Phys. Rev. B **69**, 035402 (2004).
[36] D. K. Choi, T. Takai, S. Erkoç, T. Halicioglu, and W. A. Tiller, J. Cryst. Growth **85**, 9 (1987).
[37] Z. Q. Wang and D. Stroud, Phys. Rev. B **42**, 5353 (1990).
[38] J. E. Angelo and M. J. Mills, Philos. Mag. A **72**, 635 (1995).
[39] C. H. Grein, J. P. Faurie, V. Bousquet, E. Tournié, R. Benedek, and T. de la Rubia, J. Cryst. Growth **178**, 258 (1997).
[40] T. Ito, K. E. Khor, and S. Das Sarma, Phys. Rev. B **41**, 3893 (1990).
[41] D. Conrad and K. Scheerschmidt, Phys. Rev. B **58**, 4538 (1998).
[42] R. Smith, Nucl. Instrum. Methods Phys. Res. B **67**, 335 (1992).
[43] M. Sayed, J. H. Jefferson, A. B. Walker, and A. G. Cullis, Nucl. Instrum. Methods Phys. Res. B **102**, 218 (1995).
[44] M. Nakamura, H. Fujioka, K. Ono, M. Takeuchi, T. Mitsui, and M. Oshima, J. Cryst. Growth **209**, 232 (2000).
[45] K. Albe, K. Nordlund, J. Nord, and A. Kuronen, Phys. Rev. B **66**, 035205 (2002).
[46] J. P. Rino, A. Chatterjee, I. Ebbsjö, R. K. Kalia, A. Nakano, F. Shimojo, and P. Vashishta, Phys. Rev. B **65**, 195206 (2002).
[47] F. H. Stillinger and T. A. Weber, Phys. Rev. B **31**, 5262 (1985).
[48] J. Tersoff, Phys. Rev. B **37**, 6991 (1988).
[49] J. Tersoff, Phys. Rev. B **39**, R5566 (1989).
[50] H. Balamane, T. Halicioglu, and W. A. Tiller, Phys. Rev. B **46**, 2250 (1992).
[51] S. J. Cook and P. Clancy, Phys. Rev. B **47**, 7686 (1993).
[52] J. Tersoff, Phys. Rev. B **41**, 3248 (1990).
[53] D. W. Brenner, Phys. Rev. B **42**, 9458 (1990).
[54] J. S. Blakemore, J. Appl. Phys. **53**, R123 (1982).
[55] *Pearson's Handbook of Crystallographic Data for Intermetallic Phases*, 2nd ed., edited by P. Villars and L. D. Calvert, (ASM International, Materials Park, Ohio, 1991), Vol. 1, pp. 1134–1135.
[56] J. Donohue, *The Structures of the Elements* (Wiley, New York, 1974).
[57] F. Reif, *Fundamentals of Statistical and Thermal Physics* (McGraw Hill, Boston, 1965).
[58] *CRC Handbook of Chemistry and Physics*, 83rd ed., edited by D. R. Lide (CRC Press, Boca Raton, FL, 2003).
[59] L. Brewer, Lawrence Berkeley Laboratory Report No. LBL-3720 (unpublished), 1977.
[60] O. Kubaschewski, C. B. Alcock, and P. J. Spencer, *Materials Thermochemistry*, 6th ed. (Pergamon Press, New York, 1993), pp. 1–27.
[61] S. Adachi, in *Properties of Gallium Arsenide*, 3rd ed, edited by M. R. Brozel and G. E. Stillman (INSPEC, London, 1996), Vol. 16, pp. 27–31.
[62] M. C. Payne, M. P. Teter, D. C. Allan, T. A. Arias, and J. D. Joannopoulos, Rev. Mod. Phys. **64**, 1045 (1992).
[63] *Smithells Metals Reference Book*, 7th ed., edited by E. A. Brandes and G. B. Brook (Butterworth-Heinemann, Oxford, 1998).
[64] *Atlas of Crystal Structure Types for Intermetallic Phases*, 2nd ed., edited by J. L. C. Daams, P. Villars, and J. H. N. van Vucht (ASM International, Materials Park, Ohio, 1991), Vol. 1–4.
[65] A. Mujica, R. J. Needs, and A. Munoz, Phys. Rev. B **52**, 8881 (1995).
[66] M. I. Baskes, S. P. Chen, and F. J. Cherne, Phys. Rev. B **66**, 104107 (2002).
[67] M. Bernasconi, G. L. Chiarotti, and E. Tosatti, Phys. Rev. B **52**, 9988 (1995).
[68] C. W. Snyder, B. G. Orr, D. Kessler, and L. M. Sander, Phys. Rev. Lett. **66**, 3032 (1991).
[69] D. J. Eaglesham, L. N. Pfeiffer, K. W. West, and D. R. Dykaar, Appl. Phys. Lett. **58**, 65 (1991).
[70] S. B. Zhang and J. E. Northrup, Phys. Rev. Lett. **67**, 2339 (1991).
[71] G. Zollo, J. Tarus, and R. M. Nieminen, J. Phys.: Condens. Matter **16**, 3923 (2004).
[72] M. Missous, in *Properties of Gallium Arsenide*, 3rd ed, edited by M. R. Brozel and G. E. Stillman (INSPEC, London, 1996), Vol. 16, pp. 679–683.
[73] E. S. Tok, J. H. Neave, J. Zhang, B. A. Joyce, and T. S. Jones, Surf. Sci. **374**, 397 (1997).
[74] J. R. Morris, C. Z. Wang, K. M. Ho, and C. T. Chan, Phys. Rev. B **49**, 3109 (1994).
[75] H. Wenzl, A. Dahlen, A. Fattah, S. Petersen, K. Mika, and D. Henkel, J. Cryst. Growth **109**, 191 (1991).
[76] R. Evans, in *Properties of Gallium Arsenide*, 3rd ed., edited by M. R. Brozel and G. E. Stillman (INSPEC, London, 1996), Vol. 16, pp. 655–661.
[77] K. P. Huber and G. Herzberg, *Molecular Spectra and Molecular Structure: IV. Constants of Diatomic Molecules* (Van Nostrand Reinhold Company, New York, 1979), Vol. 4.
[78] J. J. Murray, C. Pupp, and R. F. Pottie, J. Chem. Phys. **58**, 2569 (1973).
[79] J. J. BelBruno, Heteroat. Chem. **14**, 189 (2003).
[80] Q-K. Xue, T. Hashizume, and T. Sakurai, Appl. Surf. Sci. **141**, 244 (1999).
[81] D. Paget, O. Pulci, M. Sauvage, Y. Garreau, L. Reining, P. Chiaradia, F. Bechstedt, and R. Pinchaux, Surf. Rev. Lett. **9**, 1497 (2002).
[82] M. Pristovsek, S. Tsukamoto, A. Ohtake, N. Koguchi, B. G. Orr, W. G. Schmidt, and J. Bernholc, Phys. Status Solidi B **240**, 91 (2003).
[83] S. Tsukamoto, M. Pristovsek, A. Ohtake, B. G. Orr, G. R. Bell, T. Ohno, and N. Koguchi, J. Cryst. Growth **251**, 46 (2003).
[84] D. J. Chadi, J. Vac. Sci. Technol. A **5**, 834 (1987).
[85] J. E. Northrup and S. Froyen, Phys. Rev. Lett. **71**, 2276 (1993).
[86] J. E. Northrup and S. Froyen, Phys. Rev. B **50**, 2015 (1994).
[87] P. Laukkanen, M. Kuzmin, R. E. Perälä, M. Ahola, S. Mattila, I. J. Väyrynen, J. Sadowski, J. Konttinen, T. Jouhti, C. S. Peng *et al.*, Phys. Rev. B **72**, 045321 (2005).
[88] D. K. Biegelsen, R. D. Bringans, J. E. Northrup, and L. E. Swartz, Phys. Rev. B **41**, 5701 (1990).
[89] Q-K. Xue, T. Hashizume, and T. Sakurai, Prog. Surf. Sci. **56**, 1 (1997).
[90] G-X. Qian, R. M. Martin, and D. J. Chadi, Phys. Rev. B **38**, 7649 (1988).
[91] K. Reuter and M. Scheffler, Phys. Rev. B **65**, 035406 (2001).
[92] W. A. Harrison, J. Vac. Sci. Technol. **16**, 1492 (1979).
[93] J. P. Harbison and H. H. Farrell, J. Vac. Sci. Technol. B **6**, 733 (1988).
[94] M. D. Pashley, Phys. Rev. B **40**, 10481 (1989).

[95] A. Ohtake and N. Koguchi, Appl. Phys. Lett. **83**, 5193 (2003).
[96] A. Ohtake, M. Ozeki, T. Yasuda, and T. Hanada, Phys. Rev. B **65**, 165315 (2002).
[97] A. Ohtake, M. Ozeki, T. Yasuda, and T. Hanada, Phys. Rev. B **66**, 209902(E) (2002).
[98] H. C. Andersen, J. Chem. Phys. **72**, 2384 (1980).
[99] D. A. Murdick, X. W. Zhou, H. N. G. Wadley, R. Drautz, and D. G. Pettifor, (Mater. Res. Soc. Symp. Proc. **859E**, JJ9.7.1, 2005), the arsenic flux used for the Tersoff potential was effectively atomic in nature rather than molecular (as was reported).
[100] K. Ohno, K. Esfarjani, and Y. Kawazoe, *Computational Materials Science: from Ab Initio to Monte Carlo Methods*, Springer Series in Solid State Sciences, Vol. 129 (Springer-Verlag, New York, 1999).
[101] C. Kittel, *Introduction to Solid State Physics*, 7th ed. (J. Wiley & Sons, New York, 1996).
[102] J. Kioseoglou, H. Polatoglou, L. Lymperakis, G. Nouet, and P. Komninou, Comput. Mater. Sci. **27**, 43 (2003).
[103] K. Ding and H. C. Andersen, Phys. Rev. B **34**, 6987 (1986).
[104] C. Roland and G. H. Gilmer, Phys. Rev. B **46**, 13428 (1992).
[105] C. Roland and G. H. Gilmer, Phys. Rev. B **46**, 13437 (1992).
[106] G. H. Gilmer and C. Roland, Appl. Phys. Lett. **65**, 824 (1994).
[107] C. H. Grein, R. Benedek, and T. de la Rubia, Comput. Mater. Sci. **6**, 123 (1996).
[108] M. H. Liang, X. Xie, and S. Li, Int. J. Mod. Phys. B **16**, 227 (2002).
[109] H. Hensel, P. Klein, H. M. Urbassek, and T. Frauenheim, Phys. Rev. B **53**, 16497 (1996).
[110] G. C. Abell, Phys. Rev. B **31**, 6184 (1985).
[111] D. G. Pettifor and I. I. Oleinik, Phys. Rev. B **59**, 8487 (1999).
[112] A. P. Horsfield, A. M. Bratkovsky, M. Fearn, D. G. Pettifor, and M. Aoki, Phys. Rev. B **53**, 12694 (1996).
[113] D. G. Pettifor and I. I. Oleinik, Phys. Rev. Lett. **84**, 4124 (2000).
[114] L. F. Mattheiss, D. R. Hamann, and W. Weber, Phys. Rev. B **34**, 2190 (1986).
[115] X. Gonze, J-P. Michenaud, and J-P. Vigneron, Phys. Rev. B **41**, 11827 (1990).
[116] R. B. Phillips, *Crystals, Defects and Microstructures: Modeling across Scales* (Cambridge University Press, New York, 2001), pp. 476–484.
[117] D. A. Murdick, X. W. Zhou, H. N. G. Wadley, and D. Nguyen-Manh, J. Phys.: Condens. Matter **17**, 6123 (2005).
[118] B. M. Axilrod and E. Teller, J. Chem. Phys. **11**, 299 (1943).
[119] T. Ito, K. E. Khor, and S. Das Sarma, Phys. Rev. B **40**, 9715 (1989).
[120] D. C. Wallace, *Thermodynamics of Crystals* (John Wiley and Sons, Inc., New York, 1972).
[121] T. Ito, J. Appl. Phys. **77**, 4845 (1995).
[122] T. Ito and K. Shiraishi, Jpn. J. Appl. Phys., Part 2 **35**, L1016 (1996).
[123] K. Nordlund, J. Nord, J. Frantz, and J. Keinonen, Comput. Mater. Sci. **18**, 283 (2000).
[124] A. Kuronen, J. Tarus, and K. Nordlund, Nucl. Instrum. Methods Phys. Res. B **153**, 209 (1999).
[125] S. Wolfram, *The Mathematica Book*, 5th ed. (Wolfram Research, Inc., Champaign, Illinois, 2004), p. 106ff.
[126] W. H. Press, *Numerical Recipes in Fortran 77: the Art of Scientific Computing*, 2nd ed. (Cambridge University Press, New York, 1996), Vol. 1.
[127] M. Finnis, *Interatomic Forces in Condensed Matter*, Oxford Series on Materials Modelling (Oxford University Press, Oxford, 2003).
[128] K. R. Lyall and J. F. Cochran, Can. J. Phys. **49**, 1074 (1971).
[129] H. J. Beister, K. Strössner, and K. Syassen, Phys. Rev. B **41**, 5535 (1990).
[130] H. J. McSkimin, A. Jayaraman, and P. Andreatch, Jr., J. Appl. Phys. **38**, 2362 (1967).
[131] O. H. Nielsen and R. M. Martin, Phys. Rev. B **32**, 3792 (1985).
[132] S. Erkoç and H. Kökten, Int. J. Mod. Phys. C **11**, 1225 (2000).
[133] K. Nordlund and A. Kuronen, Nucl. Instrum. Methods Phys. Res. B **159**, 183 (1999).